Dual-mode CO_2-laser/microwave-sideband spectrometer with broadband and saturation dip detection for CH_3OH

Zhen-Dong Sun, Qiang Liu, R. M. Lees,[a] and Li-Hong Xu
Canadian Institute for Photonic Innovations and Department of Physical Sciences, University of New Brunswick, Saint John, N.B. E2L 4L5, Canada

M. Yu. Tretyakov and V. V. Dorovskikh
Institute of Applied Physics of Russian Academy of Sciences, 46 Ulianov Str., Nizhnii Novgorod, Russia 603950

(Received 9 October 2003; accepted 5 January 2004; published 16 March 2004)

This work reports dual-mode operation of a broadly tunable CO_2-laser/microwave-sideband spectrometer employing a Cheo waveguide modulator and a CO_2 laser that can operate on hot and sequence band lines as well as low- and high-J regular band lines. The spectrometer has a broadband scanning mode at Doppler-limited resolution for spectral searching and assignment, and a narrow-band sub-Doppler mode for precision measurements. In broadband mode, a 6.7–18.5 GHz ($\sim$0.4 cm^{-1}) window can be covered for each sideband in a single microwave sweep with a tracking Fabry–Perot etalon filter under computer control. In sub-Doppler mode, saturation-dip spectra are obtained at sub-MHz resolution with absolute frequency measurement accuracy of the order of $\pm$200 kHz. The instrumental performance is demonstrated via spectra of the C–O stretching fundamental vibrational band of methanol. Doppler-limited broadband scans have been recorded with good signal-to-noise ratio in both the low- and high-J regions of the 9.6-μm-CO_2 laser band, while narrow-band sub-Doppler scans have permitted clean separation of very close-lying lines in the CH_3OH spectrum. The measurement precision is confirmed for several CH_3OH transition systems through closure of combination loops. Our results illustrate the wide coverage and excellent resolution obtainable with CO_2-sideband infrared laser radiation in a broadly tunable and convenient infrared source with high potential for spectroscopic applications. © *2004 American Institute of Physics.* [DOI: 10.1063/1.1651636]

I. INTRODUCTION

In the 10-μm-midinfrared region, sideband generation by mixing CO_2 laser and microwave (MW) radiation in an electro-optic modulator has provided one of the best available sources of widely tunable infrared (IR) radiation of precisely known frequency.[1–6] The accessible tuning range has generally extended from 8–18 GHz on either side of each CO_2 laser line for the GaAs waveguide modulators developed by Cheo,[1–3] and from 12–18 or 8–18 GHz for the CdTe modulators developed originally by Magerl.[4] While this coverage is good, there are still significant gaps when only the regular CO_2 laser bands are available, because the spacing between the regular CO_2 lines varies from about 70 to 20 GHz going from P to R branch across a band. However, by innovative design of the mechanical and optical structures, Evenson *et al.* developed a cw CO_2 laser with particularly high resolution that could operate with significant power on many of the lines of the CO_2 hot and sequence bands.[7] Accurate frequencies for these lines were measured and tabulated by Maki *et al.* for several CO_2 isotopomers.[8] Since the hot and sequence band lines serve to bridge many of the gaps between the regular band lines, there is considerable advantage in spectral coverage if these additional CO_2 laser lines can be used as well for microwave sideband generation.

Recently, we described the assembly of a CO_2-laser/microwave-sideband tunable infrared source[9] employing an Evenson laser and a Cheo waveguide modulator,[1,2] for application in spectroscopic measurements. In the present work, we report significant extensions to our system and development of its capabilities as a dual-mode precision computer-controlled spectrometer. In the first, broadband scan mode we have employed hot and sequence band CO_2 laser lines interspersed among the regular lines of the 9.6 μm band from $9P4$ to $9R6$ to achieve almost complete tunability over this difficult low-J region for application in broadband spectroscopy in the Doppler-limited regime. We have also utilized the extended tuning range of the laser to generate sidebands for laser lines from $9P42$ to $9P56$ in the high-J wing of the 9.6-μm-P branch. In the second, sub-Doppler mode of the spectrometer, a rearrrangement of the optical layout permits spectral measurements at sub-MHz resolution employing saturation-dip detection. In both modes of operation, the scans are now automated under computer control, with a tracking scheme for tuning the high-finesse Fabry–Perot (FP) etalon filter for sideband separation.

As an application to highlight the features and capabilities of our spectrometer, we have recorded spectra of the ν_8 vibrational C–O stretching fundamental band of methanol

[a]Author to whom correspondence should be addressed; electronic mail: lees@unb.ca

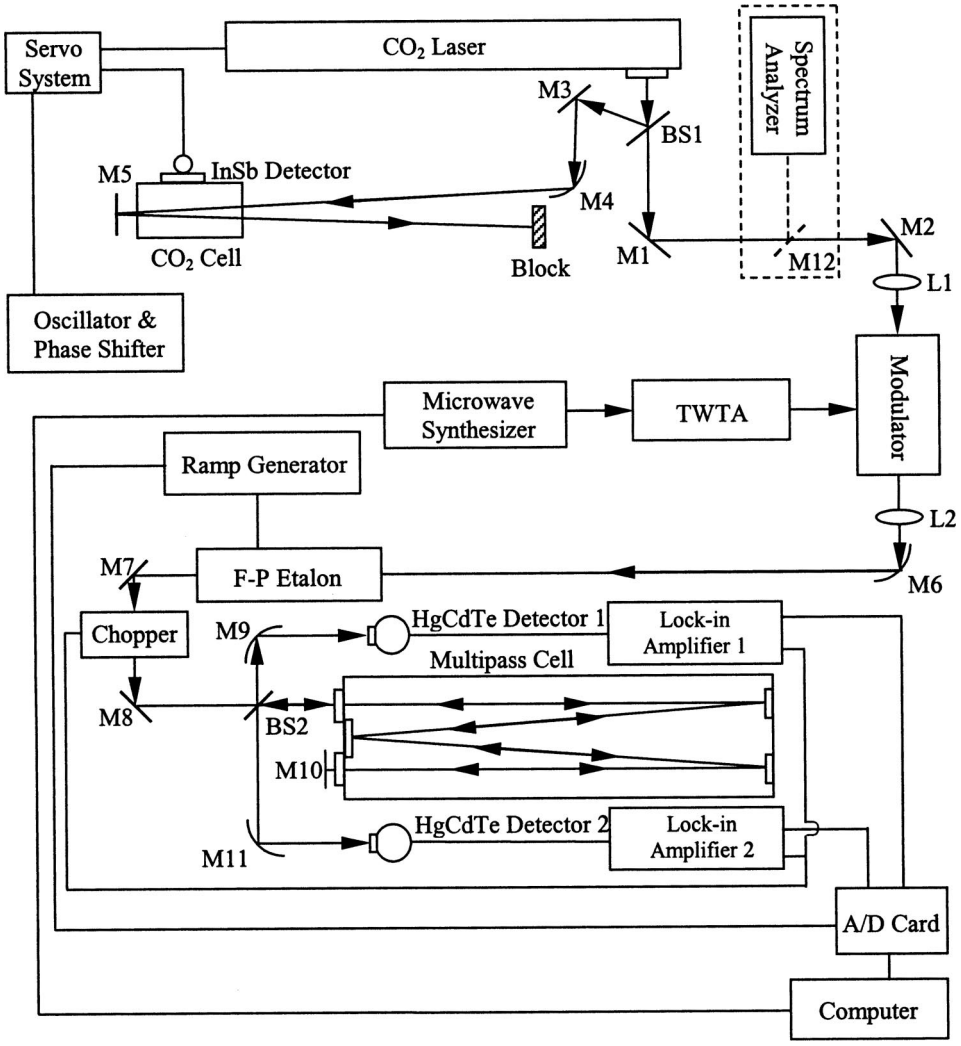

FIG. 1. Block diagram of the tunable CO_2-laser/microwave-sideband spectrometer in the broadband Doppler-limited mode. BS1, BS2 beam splitters; L1, L2, ZnSe lenses; M1–M12, mirrors (M4, M6, M9, and M11 are concave); TWTA, traveling wave tube amplifier; FP, tunable Fabry–Perot etalon filter.

utilizing each of the instrumental modes. Both the low-J range from $9P4$ to $9R6$ and the high-J range from $9P42$ to $9P56$ were covered with a series of full-sideband scans in the Doppler-limited regime. In both spectral regions, we then recorded narrow-band sub-Doppler scans for a number of close-lying CH_3OH lines that are overlapped and unresolved in high-resolution Fourier transform (FT) spectra. A clean separation is afforded by the Lamb-dip observations with high accuracy of measurement.

II. CO_2-LASER/MICROWAVE-SIDEBAND SPECTROMETER

A. Instrumental details for the broad-scan mode

A block diagram of the spectrometer as set up for the first mode of operation in the broad-scan Doppler-limited regime is shown in Fig. 1. We will outline the source details briefly and refer to our previous report[9] for additional description. The tunable CO_2-laser/microwave infrared sidebands are generated in a Cheo-type CdTe-buffered GaAs waveguide microwave modulator (PC Photonics).[1] The grating-tuned CO_2 laser (frequency f_L) is of Evenson manufacture[7] and is operated at a dc bias voltage of 13 kV and a tube current of 12 mA in each leg. Flowing premixed gas (Air Liquide, Inc.) consisting of 16.2% N_2, 12% CO_2 and the balance He is used in the laser at an inlet pressure of ~25 Torr. The laser power (measured with a Thorlabs D30MM-X power meter) is in the range from 1 to 10 W depending on the particular line, with a spot size of ~5 mm in diameter. The desired laser line is selected using a previously determined calibration curve giving the setting of the grating micrometer versus laser line for both the regular bands and the hot and sequence bands. The line selection is then checked with a CO_2 spectrum analyzer (Optical Engineering, Inc.).

For frequency stabilization, 20% of the laser power is split off to lock the laser to the zero crossing of the 4.3-μm-fluorescence Lamb-dip error signal from an external CO_2 cell (at a gas pressure of ~40 mTorr), detected by a liquid-nitrogen-cooled InSb detector. The traditional first-derivative servo technique is used,[10] with a 1 kHz signal applied to the laser piezotuning element (PZT) in order to modulate the cavity length and thereby the laser frequency. From the fluctuations in the error correction voltage, we estimate the frequency accuracy of the locked laser frequency to be of the

order of ±100 kHz. For the hot and sequence band laser lines and also the high-J $9P54$ and $9P56$ regular lines, their lower power is currently insufficient for Lamb-dip locking, hence the laser is first adjusted to the peak of the gain curve and then swept while in the free-running state. For the 6.7–18.5 GHz broadband scans with 2 MHz step size, where the scan time is around 10 min, we estimate that the typical free-running drift should not exceed 5 MHz. For the few-MHz narrow-band high-resolution saturation-dip scans discussed in Sec. II B, the scans are of much shorter duration and we estimate a maximum drift of 0.5 MHz.

After passing through a two-mirror polarization rotator, the main 80% beam is focused into the modulator by a ZnSe lens of 10 cm focal length. Microwave radiation (frequency f_{MW}) in the range 6.7–18.5 GHz is generated by a microwave synthesizer (Hewlett Packard 83630A) and amplified to a power of ~15 W by a traveling-wave-tube amplifier (CPI Model ZM-6991K4ADE). It is then fed to the modulator through a 10-cm-low-loss coaxial cable (Astrolab Minibend-4) and mixed with the CO_2 radiation to generate the laser sidebands. The output MW port from the modulator is terminated with a 20-W-matched load (Midwest Microwave TRM-2129-F0-SMA-07).

The radiation emerging from the exit window of the modulator contains the laser carrier f_L and two sidebands at frequencies $f_L \pm f_{\mathrm{MW}}$. The desired sideband is separated from the carrier by a high-finesse tunable Fabry–Perot etalon filter (Burleigh TL15-0075-FIR) having balanced PZT elements controlled by a three-channel, 0–1000 V ramp generator (Burleigh RG-93). The etalon has mirrors of ~97.5% reflectivity and a free spectral range of 75 GHz, corresponding to a finesse of ~63 and a passband of ~1.2 GHz. The typical transmission efficiencies (ratio of the output power to the input power) of the modulator and FP filter were measured to be ~25% and ~30%, respectively. In order to determine the sideband conversion efficiency, the FP filter was scanned through both sideband and carrier frequencies and the relative powers were monitored with a pyroelectric detector.[9] From the heights of the detector signals observed on an oscilloscope, the conversion efficiency (P_s/P_c) was found to be ~0.6%, where P_s and P_c are, respectively, the sideband and carrier powers at the output from the FP filter.

Following the FP filter, the selected CO_2 laser sideband is amplitude modulated by an optical chopper (Stanford Research Systems SR540) at a frequency of just above 1 kHz before being split in a 7:3 ratio into a signal beam and a reference background beam. Two liquid-nitrogen-cooled HgCdTe detectors simultaneously detect the background beam and the signal beam after the latter has transitted our gas sample cell (Model 35-V, Infrared Analysis, Inc.). This is a 60-cm-White-type multipass cell, employing mirrors with protected gold coating, that we fitted with ZnSe windows. The double-pass arrangement shown in Fig. 1 was used, in which mirror M10 returns the signal beam back through the cell to double the total absorption path length but with the angle slightly offset in order to avoid fringing effects. When the signal radiation re-emerges from the cell, it is reflected off beamsplitter BS2 onto concave mirror M11 and focused into detector 2. The two detected signals are demodulated by identical lock-in amplifiers (Stanford Research Systems SR510) operating in $1f$ mode, and sent via an A/D card to the computer where their ratio is calculated. This sample-to-background ratio procedure greatly improves the signal-to-noise (S/N) ratio of the molecular absorption signals and gives a relatively flat background over the 6.7–18.5 GHz range of a scan. The procedure effectively compensates both for random fluctuations in the laser sidebands as well as for systematic power variations as a function of frequency due principally, we believe, to standing waves in the microwave circuitry.

Within the region of the six low-J CO_2 laser lines from $9P4$ to $9R6$ in the center of the 9.6 μm band, we also observed three hot band (H) and three sequence band (S) lines interspersed among the regular lines. The typical output power of the H and S lines is ~1 W, as compared to a typical output power of ~6 W for the regular lines. By using each of the 12 laser lines to generate sidebands, we are able to cover most of the gaps between the regular band lines and obtain near-continuous spectral coverage from 1059.95 cm^{-1} ($9P4-18.5\,\mathrm{GHz}$) up to 1069.63 cm^{-1} ($9R6+18.5\,\mathrm{GHz}$), a range of almost 10 cm^{-1}. Figure 2 depicts several examples of our broadband scans for the C–O stretching band of CH_3OH. The top axes give the MW sideband frequencies (GHz) and the bottom axes give the absolute wave numbers (cm^{-1}). Regions where the spectra overlap are labeled by corresponding numbers (①–①,②–②) and show good comparability. The 10 cm^{-1} window extends over eight consecutive J multiplets in the CH_3OH C–O stretching R branch, representing a respectable coverage for the purposes of spectroscopic assignment.

In the high-J regime, the CH_3OH spectrum was scanned using sidebands from the $9P42$ to $9P56\,CO_2$ lines. Examples of the spectral recordings are presented in Fig. 3. Here, the laser could be locked to the Lamb dip up to $9P52$, but was free-running for the lower power $9P54$ and $9P56$ lines after being initially tuned to the peak of the gain curve at the start of each scan, as discussed above at the beginning of this section.

B. Operation in saturation-dip mode at sub-MHz resolution

The second mode of operation of our spectrometer involves narrow-band scans at sub-Doppler resolution in order to record standard reference spectra at high accuracy and to resolve very close lines that are blended in Doppler-limited spectra. Two main modifications were made to the optical arrangement of Fig. 1 in order to realize saturation-dip observations. First, mirror M10 in Fig. 1 was reoriented to act as a precise retroreflector in order to return the radiation incident on the cell back along exactly the same path.[11] This gives the counterpropagating overlapping beams inside the cell that are a prerequisite for observation of Lamb dips. The second crucial change was to move the FP filter from its location in front of the absorption cell to a position following the cell, between mirror M11 and detector 2. This allows much higher sideband power to reach the cell from the modulator and gives effective saturation of the molecular

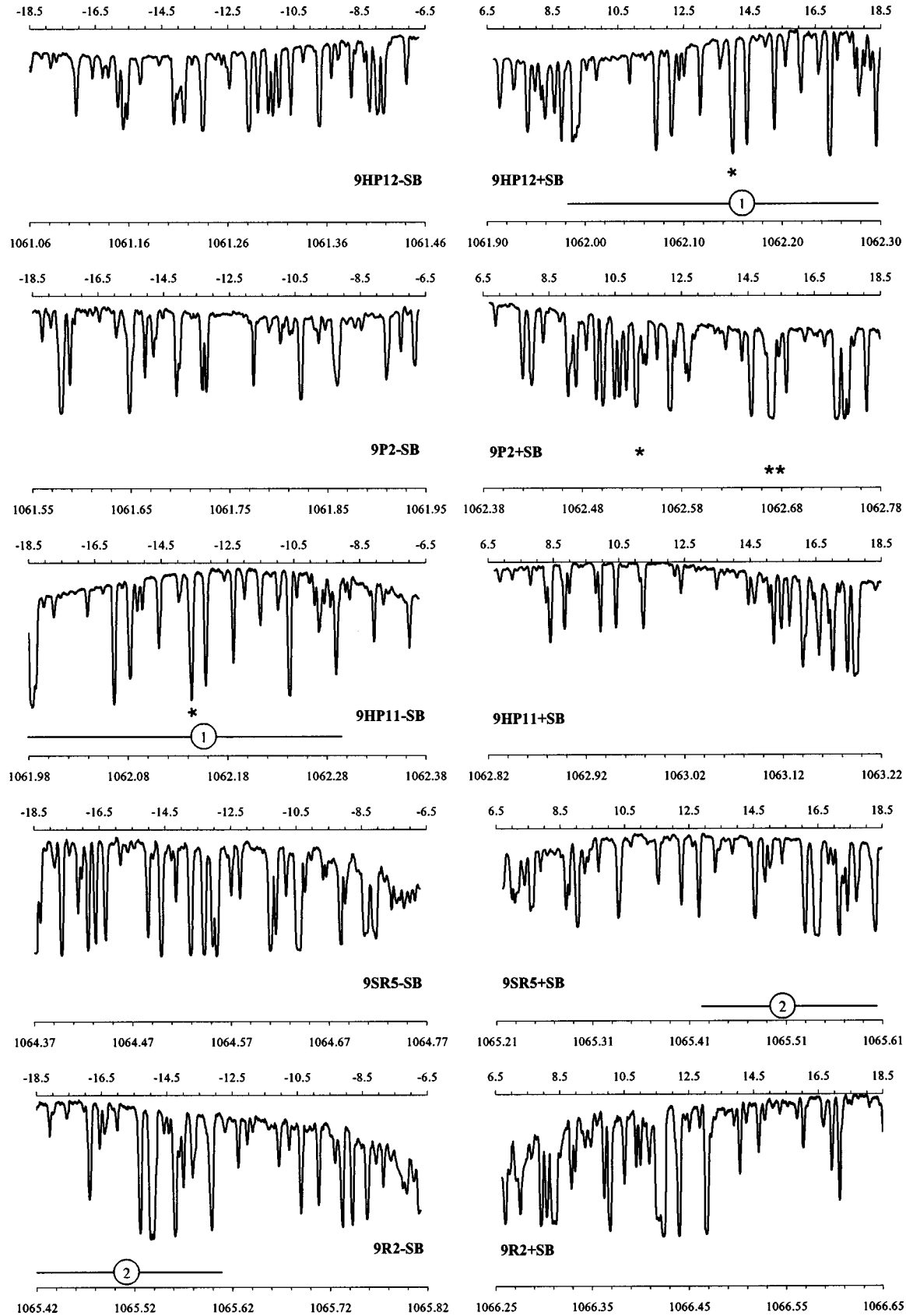

FIG. 2. Examples of broadband spectra of the C–O stretching fundamental band of CH_3OH recorded in Doppler-limited mode using microwave sidebands of hot, sequence, and low-J regular band CO_2 laser lines. Each segment represents a continuous scan over a full microwave sideband from 6.7 to 18.5 GHz. The lines marked with (*) or (**) in the $9P2$, $9HP11$, and $9HP12$ sideband spectra were also scanned at sub-Doppler resolution, as shown in Figs. 6 and 7 and discussed in Sec. III B. Overlapping regions of the spectrum are labeled as ①–① and ②–②.

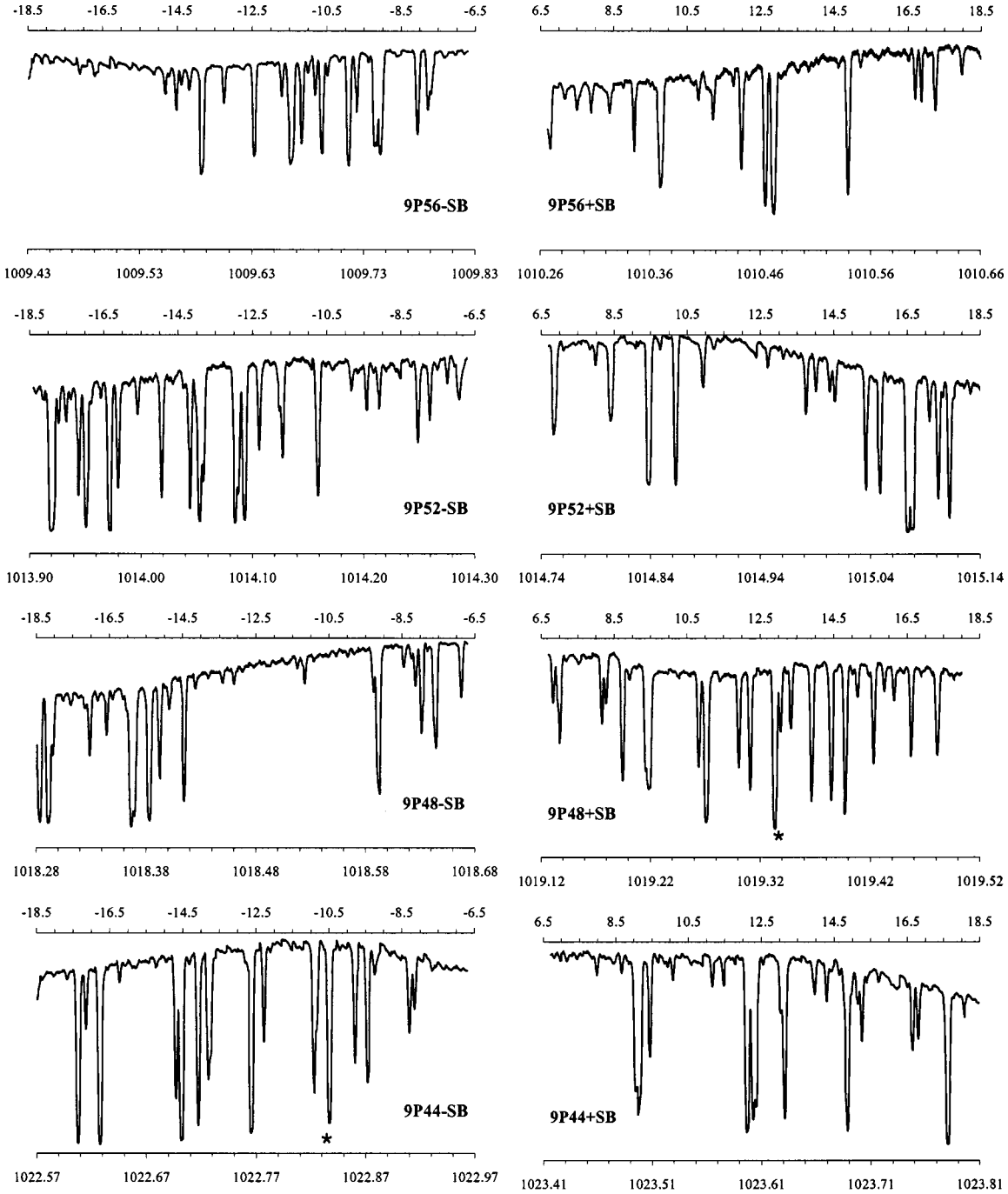

FIG. 3. Examples of broadband sideband spectra of the C–O stretching fundamental band of CH_3OH recorded in Doppler-limited mode using high-J P-branch lines of the regular 9.6-μm-CO_2 laser band. The lines marked with (*) were also scanned at sub-Doppler resolution, as shown in Figs. 4 and 5 and discussed in Sec. III B.

absorption. (However, since the radiation reflected off the front surface of BS2 now contains both carrier and sideband, we can no longer monitor the background sideband power via detector 1, so mirror M9 is replaced by a beam block.) For spectral observations, we could take advantage of the 1 kHz frequency modulation of the CO_2 laser already provided by the laser-locking system. With just the single detection channel, we also switched to a digital lock-in amplifier (Stanford Research Systems SR830) to have the capability for operating in either the $2f$ or $3f$ mode for detection of the infrared spectral signals. We find that $3f$ detection is effective in giving a reasonably flat baseline for scans over a few tens of MHz with a single detector.

C. Operational details and computer-control procedures

During operation of the sideband spectrometer, the frequency and power output of the microwave synthesizer, the tuning of the FP filter PZT elements by the ramp generator voltage, and the data acquisition from the lock-in amplifiers are all computer controlled via a program written in Visual

C^{++}. The program class structure was developed to control each device separately as well as provide total control of the experiment. The object-oriented approach allows ready extensions and further improvements to the program.

The synthesizer output power is varied during a sweep to compensate for the frequency dependence of the TWTA gain and maintain the power level at the modulator as close to 15 W as possible over the range of the sweep. A power calibration curve was determined in advance by measuring the output from the TWTA at a comb of points across its range using a microwave power meter (Hewlett Packard 435B) equipped with a high-power probe (Hewlett Packard 8481B). The data were then stored in the computer as a lookup table. The program uses a spline-approximated function of the calibration data to determine the best power value for each frequency. Communication with the synthesizer is via the GPIB bus, whereas a 16-bit multifunction D/A card (National Instruments PCI-6035E) transmits the analog tuning voltage to the ramp generator for adjustment of the FP filter and also reads and digitizes the analog signal from the lock-in amplifier. During the source frequency scan, the spectrum is displayed in real time on the computer monitor.

In implementing the broadband scanning mode of our instrument, the automated tracking of the FP PZT voltage to keep the filter passband centered on the sideband frequency forms an integral part of the process. To set up a scan with computer control of the FP resonator length, our program requires settings for the initial start frequency, the sign of the sideband, the MW scan direction and the starting voltage for optimum FP tuning. This last parameter varies for different CO_2 carrier lines and can change somewhat even for the same CO_2 line at different times due to temperature fluctuations and the well known hysteresis of the PZT. Thus, there is provision in the program for adjustment of the FP filter tuning from the computer keyboard at the beginning of a scan in order to optimize the sideband signal observed on an oscilloscope monitoring the detector output. Then, in order to maintain this maximum sideband transmission as the microwave frequency is swept during the scan, the FP response is tracked accordingly.

In our automation program, two alternative schemes have been built in to accomplish this ''synchronization.'' In the first approach, the PZT voltage V is changed by a given ''voltage step size'' after each MW frequency increment of $N\Delta f$, where Δf is the frequency step size and N is the number of steps in an increment. The size of the frequency increment is set by the operator in response to the query ''Change voltage every...GHz'' in the interactive control dialog of the program window interface. This scheme is readily comprehensible and in principle is easy to implement. If one had a good idea of the numerical relation between the FP cavity length, i.e., the filter frequency, and the PZT tuning voltage, then one could just employ a tuning curve or a look-up table stored in the computer to adjust the FP filter. In practice, due to temperature fluctuations, PZT hysteresis, and the nonlinear relation between the passband frequency and PZT voltage, this control scheme can follow the changing sideband frequency only very roughly and the sideband can sometimes be lost during a broadband scan.

The second method is more sophisticated in that the FP resonator length is adjusted close to ''real time'' and more accurately follows the scan frequency, although requiring extra data acquisition time. The algorithm employs a ''leapfrog'' approach by jumping the peak of the FP filter curve ahead of the sideband frequency by a prescribed amount after each frequency increment $N\Delta f$, so that the sideband sweep will then pass through the peak during the following increment. As above, in each increment the program makes a number N of frequency substeps Δf corresponding to the input ''Change voltage every...GHz'' value, with V held constant. After an increment is completed, the frequency sweep pauses to allow automatic adjustment of the FP filter PZT voltage at that fixed frequency. The program first takes a voltage step back by an amount ΔV determined by the ''voltage step size'' (thus detuning the FP filter and leading to a signal decrease) and measures the sideband output signal y_1. It then steps the voltage forward, with the signal now increasing, until the output signal reaches a maximum $y_{\max}$ and starts to decrease. The program continues stepping the voltage until the output signal drops to a specified percentage $P\%$ of the maximum, as set initially by the operator in the ''adjust to ...%'' parameter control dialog. The sequence of steps is: $(-\Delta V,y_1)$, $(\Delta V,y_2)$, $(\Delta V,y_3)\ldots(\Delta V,y_{\max})\ldots(\Delta V,P\%*y_{\max})$. With this scheme, the synchronization between the FP resonator tuning and the scan frequency is adjusted on a real-time automated basis, with the FP filter leapfrogging over the sideband at each adjustment step. In principle, by reducing the frequency increment in the ''Change voltage every...GHz'' command and increasing $P\%$, the tracking can be held as close as desired (subject to a minimum voltage step size determined by the digital resolution of the D/A card) at the expense of increased scan time.

With this scheme, a small discontinuity can occur in the detected signal when the FP filter is retuned at the end of a frequency increment and the transmission makes a discrete change back to $P\%$ in resetting the filter for the next increment. In order to avoid having such a tuning jump possibly appear in the middle of an absorption line, a special function was introduced in the scan program to allow the operator to intervene manually to pause the sweep and initiate a tuning correction at any point. Thus, when watching the spectrum on the computer monitor as the scan nears the end of an increment, the operator can choose to initiate the next correction when the signal is still close to the baseline, rather than being halfway up an absorption line at the end of the increment.

The main difference between the two FP control schemes is summarized here. In the first scheme, the PZT voltage is adjusted to give the maximum sideband power prior to the start of the frequency scan and thereafter is controlled according to a slope value $\Delta V/(N\Delta f)$ supplied in advance by the user. No further sideband power maximization search is performed during the scan. In the second control scheme, on the other hand, the sideband power maximum is located automatically after every $N\Delta f$ frequency increment. The FP voltage then overshoots in steps ΔV until a prescribed percentage $P\%$ of the maximum sideband

power transmission is reached, with the value of $P\%$ specified by the user. Typically, voltage steps of $\Delta V = 1$ V and frequency increments $N\Delta f = 300$ MHz were used in control scheme 2. In our broadband scans described below, a step size of $\Delta f = 2$ MHz was used.

In the narrow-band saturation-dip mode of the spectrometer, the sweep range is generally much less than the passband of the FP filter, so that tracking of the filter is not essential. Thus, one only needs to carry out an initial PZT voltage adjustment via the computer keyboard in order to center the peak of the FP filter transmission curve on the sideband frequency prior to a scan.

III. DUAL MODE OBSERVATIONS OF THE C–O STRETCHING SPECTRUM OF CH_3OH

A. Broadband scans in the Doppler-limited regime

Figures 2 and 3 show examples of the spectra that we have obtained for CH_3OH in the broadband spectrometer mode with full-sideband sweeps at Doppler-limited resolution. The spectra were recorded using a typical CH_3OH pressure of 80 mTorr with a lock-in time constant of 0.3 s and an absorption path length of 9.6 m. Each chart represents a continuous scan of microwave frequency over the full sideband width from 6.7 to 18.5 GHz. The step size for the sweeps was 2 MHz per point. It is seen in Fig. 2 that the laser sidebands for the sequence and hot band CO_2 lines, despite the lower laser power, give spectra quite comparable to those for the regular band lines. This can be checked in the overlap regions where the same spectral lines are covered by sidebands generated by different CO_2 laser lines. For example, the $9HP11$ lower sideband has a region of overlap with the $9HP12$ upper sideband (①–①), while the $9R2$ lower sideband overlaps with the $9SR5$ upper sideband (②–②). The spectra in these overlapping regions display the same lines in Fig. 2 with very similar relative intensity patterns. This confirms that the hot and sequence band CO_2 laser lines have indeed been correctly identified, and confirms the good performance of the system even with these weaker CO_2 lines.

B. High-resolution saturation-dip observations

To extend the database of precise measurements[3,12–14] for the C–O stretching band of CH_3OH, we carried out a number of Lamb-dip observations in both the high- and low-J regions of the P branch of the 9.6-μm-CO_2 laser band. Our study focused primarily on broader features that are blended in our broadband and the literature FT spectra, in order to improve the measurement accuracy significantly and sort out precise identifications for features associated with multiple transitions in the literature. Assignments and measured frequencies were determined for 33 transitions altogether, and are shown in Table I. For each line, the transition frequency was obtained by least-squares fitting the experimental data points to the appropriate derivative of a Gaussian line shape using ORIGIN software. For methanol, the energy levels can be specified by the set of quantum numbers $(\upsilon_t\,\mathrm{TS}\,K,J)^{\upsilon}$, where υ_t is the torsional quantum number, TS is the torsional A or E symmetry, K is the axial projection of rotational angular momentum J, and υ is the vibrational mode. The excited C–O stretching state is denoted by $\upsilon = \mathrm{CO}$, and the ground state by $\upsilon = \mathrm{gr}$.[15] In the figures and Table I the C–O stretching band transitions are labeled using υ_t, K, TS, $R/P(J)$.

TABLE I. Observed saturation-dip frequencies for transitions in the ν_8 C–O stretching fundamental band of CH_3OH.

Transition				CO_2 laser line±	
υ_t	K	TS	$R/P(J)$	MW sideband (MHz)[a]	ν_{obs}[b] (cm^{-1})
0	−10	E	$R(19)$	$9P2+15\,243.43$	1062.674 431
0	1	A^-	$R(19)$	+15 193.64	1062.672 770
0	3	A^-	$R(19)$	+15 116.54	1062.670 199
1	−3	E	$R(19)$	+11 110.46	1062.536 570
0	−4	E	$R(19)$	+11 098.44	1062.536 169
0	4	A^+	$R(18)$	−17 599.00	1061.578 926
0	4	A^-	$R(18)$	−17 616.59	1061.578 339
0	1	E	$R(19)$	$9HP12+13\,975.04$	1062.147 081
1	1	A^-	$P(6)$	$9P44+12\,338.71$	1023.600 950
0	4	E	$P(6)$	+12 251.72	1023.598 048
0	1	E	$P(6)$	+12 091.13	1023.592 692
0	2	A^-	$P(6)$	+9133.67	1023.494 041
0	2	A^+	$P(6)$	+9060.24	1023.491 592
0	−3	E	$P(6)$	+9037.35	1023.490 829
1	4	E	$P(7)$	−10 455.47	1022.840 618
1	2	A^+	$P(7)$	−10 465.39	1022.840 287
1	2	A^-	$P(7)$	−10 475.98	1022.839 934
2	4	A	$P(8)$	−13 783.47	1022.729 608
0	3	A^+	$P(8)$	$9P46-7475.84$	1020.807 545
0	3	A^-	$P(8)$	−7480.27	1020.807 397
0	−2	E	$P(8)$	−10 930.11	1020.692 323
0	−4	E	$P(8)$	−10 947.69	1020.691 736
0	1	A^+	$P(8)$	−13 549.56	1020.604 947
1	5	E	$P(8)$	−13 554.03	1020.604 798
1	2	A^+	$P(9)$	$9P48+12\,887.21$	1019.330 564[c]
1	4	E	$P(9)$	+12 886.36	1019.330 536[c]
1	2	A^-	$P(9)$	+12 863.57	1019.329 776
0	−5	E	$P(8)$[d]	+12 205.44	1019.307 823
0	2	A^-	$P(9)$	−18 141.74	1018.295 555
0	2	A^+	$P(9)$	−18 377.92	1018.287 672
0	3	A^+	$P(10)$	$9P50+16\,708.87$	1017.278 290
0	3	A^-	$P(10)$	+16 695.28	1017.277 836
0	−4	E	$P(10)$	+13 214.68	1017.161 736

[a]Accuracy of the sideband frequencies is estimated to be ±0.20 MHz, except for the measurement made with the free-running $9HP12$ laser line for which the estimated accuracy is ±0.5 MHz.
[b]Frequencies are converted to wave number using the conversion factor 29 979.2458 MHz/cm^{-1}; CO_2 laser frequencies are from Ref. 8.
[c]Closest overlapping lines resolved in this work.
[d]Lower component of a transition doublet hybridized by Fermi resonance between $K=-5E$ $\upsilon_t=0$ levels of the C–O stretching state and the $K=-5E$ $\upsilon_t=3$ levels of the ground state (see Ref. 15).

The great advantage of the saturation-dip detection mode is the ability to resolve very close lines in the spectrum. Figure 4 shows a recording with the $9P44$ laser line in which the components of the $P(7)K=2A$ asymmetry doublet in the excited $\upsilon_t=1$ torsional state as well as the nearby $P(7)K=4E$ $\upsilon_t=1$ line are all clearly resolved. Here, it can be seen that the use of the $3f$ detection mode of the lock-in amplifier effectively removes background variations and gives a flat baseline. The approach to the limiting resolution of the spectrometer is illustrated in Fig. 5 for the very close

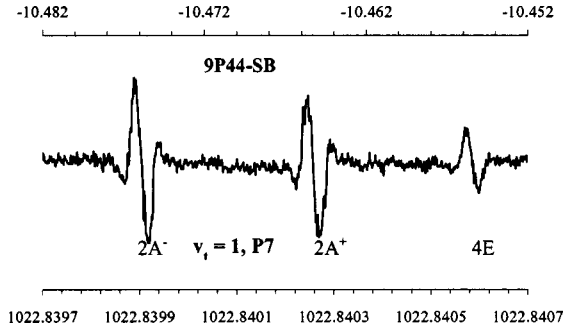

FIG. 4. Saturation-dip sub-Doppler spectra of the $P(7)K=2A$ $\upsilon_t=1$ asymmetry doublet and the nearby $P(7)K=4E$ $\upsilon_t=1$ transition of CH_3OH, recorded with the lower sideband of the $9P44\,CO_2$ laser line. The spectra were recorded using the $3f$ detection mode of the lock-in amplifier, with a time constant of 30 ms and a methanol pressure of 10 mTorr.

$P(9)$ lines of the $K=4E$ and $2A^+$ $\upsilon_t=1$ subbands, recorded in $3f$ mode using the $9P48\,CO_2$ line. The two lines are only 0.85 MHz apart hence their profiles overlap in Fig. 5, but it is unmistakable that there is more than one transition present. The dashed lines show third-derivative Gaussian profiles fitted to the experimental data with vertical bars indicating the line centers. Turning to the low-J CO_2 laser region, in Fig. 6 we show two plots of CH_3OH Lamb-dip signals recorded in $3f$ mode using the upper sideband of the $9P2$ laser line. The original overlapped spectral features (*) and (**) in Fig. 2 have now been clearly resolved in Figs. 6(a) and 6(b) into two and three constituent lines, respectively.

With careful system alignment and tuning, we were also able to obtain saturation-dip signals with the weak hot band lines. A recording is shown in Fig. 7 of a Lamb dip observed using the upper sideband of the $9HP12\,CO_2$ laser line. The signal corresponds to the strong, single Doppler-broadened line marked with an asterisk in Fig. 2, which is the $R(19)K=1E$ $\upsilon_t=0$ transition. Here, the laser was not locked but initially set to the peak of the gain curve. However, there is little laser drift during the relatively short duration of the narrow-band Lamb-dip scan, and we estimate the accuracy

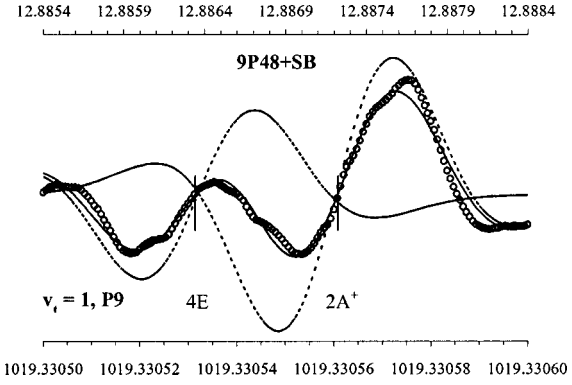

FIG. 5. Saturation-dip sub-Doppler spectrum of the blended $P(9)$ $K=4E$ and $2A^+$ $\upsilon_t=1$ transitions of CH_3OH, recorded with the upper sideband of the $9P48\,CO_2$ laser line using $3f$ mode with 0.1 s time constant. The solid line represents a least-squares fit to the experimental data points (open circles) employing third derivatives of two overlapping Gaussian profiles, shown individually by the dashed curves. The two vertical bars show the line centers.

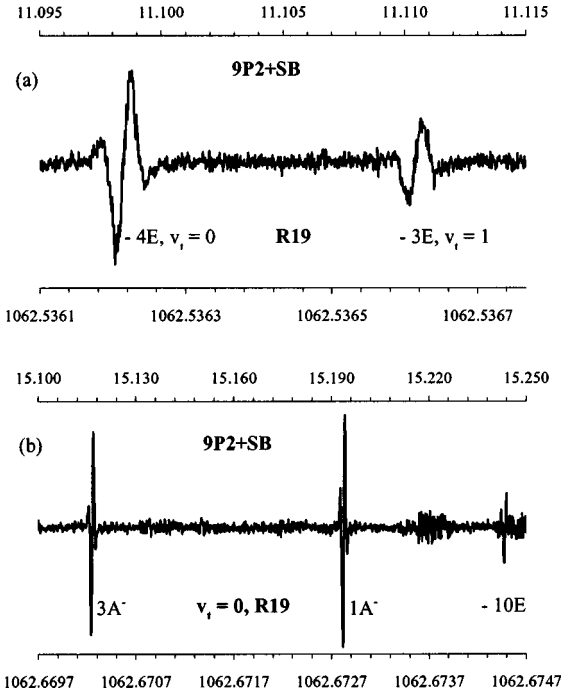

FIG. 6. Saturation-dip sub-Doppler spectra of CH_3OH observed using the upper sideband of the $9P2\,CO_2$ laser line. Trace (a) with 20 MHz span corresponds to the blended line marked (*) in Fig. 2 that includes the $K=-4E$ $\upsilon_t=0$ and $-3E$ $\upsilon_t=1$ absorptions in the $R(19)$ multiplet. Trace (b), with 150 MHz span, corresponds to the blended feature marked (**) in Fig. 2 and includes the $R(19)$ $K=3A^-$, $1A^-$, and $-10E$ $\upsilon_t=0$ absorptions. Both spectra were recorded using $3f$ detection, with a lock-in time constant of 30 ms and a methanol pressure of 10 mTorr.

of the measurement to be ± 0.5 MHz. The open circles represent the data points for the individual scan steps, and the solid line is a second-derivative Gaussian profile fitted to the observed data.

In least-squares fitting of each of the observed Lamb-dip signals to a second- or third-derivative Gaussian profile, the accuracy of determination of the transition peak frequencies is better than ± 100 kHz. Coupled with the ± 100 kHz uncertainty in the frequency of the locked laser, this gives a total estimated measurement uncertainty for the Lamb-dip obser-

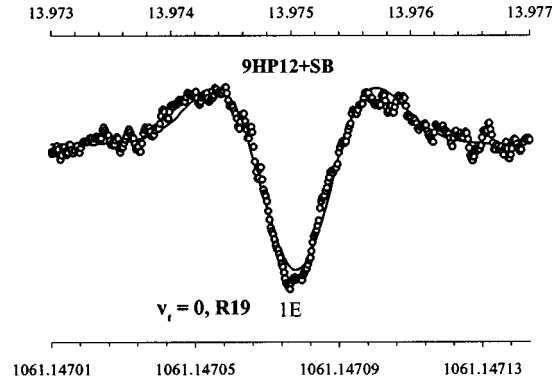

FIG. 7. Saturation-dip sub-Doppler spectra of the $R(19)$ $K=1E$ $\upsilon_t=0$ transition of CH_3OH [marked (*) in Fig. 2] taken with the upper sideband of the $9HP12\,CO_2$ laser line. The spectrum was recorded using $2f$ detection, with a lock-in time constant of 30 ms and methanol pressure of 8 mTorr. The solid curve is a least-squares fit of a second-derivative Gaussian profile to the experimental data points (open circles).

vations of the order of ±200 kHz. This estimate can be supported by applying the Ritz combination principle to closed loops of transitions using known Lamb-dip IR and ground-state millimeter-wave data[3,16] along with the CO_2 laser frequencies given by Maki *et al.*[8] and the results observed here. For the $K=2A\ \upsilon_t=1$ asymmetry-doublet system with the $9P44$ line in Table I, two loop closure relations can be checked (with the frequencies given in MHz):

$$(1A2^+,7)^{gr}\rightarrow(1A2^+,6)^{Co}\rightarrow(1A2^+,5)^{gr}\rightarrow(1A2^+,6)^{gr}\rightarrow(1A2^+,7)^{gr}$$
$$=[9P44-10\,465.39]-[9P24+17\,773.04]+289\,414.030+337\,625.679=-0.10$$
$$(1A2^-,7)^{gr}\rightarrow(1A2^-,6)^{co}\rightarrow(1A2^-,5)^{gr}\rightarrow(1A2^-,6)^{gr}\rightarrow(1A2^-,7)^{gr}$$
$$=[9P44-10\,475.98]-[9P24+17\,778.63]+289\,420.240+337\,635.655=-0.09.$$

For the $K=5E\ \upsilon_t=1$ system with the $9P46$ laser line, the closed-loop combination relation is

$$(1E5,8)^{gr}\rightarrow(1E5,7)^{co}\rightarrow(1E5,6)^{gr}\rightarrow(1E5,7)^{gr}\rightarrow(1E5,8)^{gr}$$
$$=[9P46-13\,554.03]-[9P22-8356.01]+337\,685.490^*+385\,958.092=0.21.$$

Note that the $J=7\leftarrow6$ millimeter frequency marked with an asterisk above is for an overlapped line. The calculated frequency for this transition in Ref. 16 is actually 337 685.218 MHz, which would bring the closure defect down to −0.07 MHz. Thus, the closure defects for the three transition combination loops are all well within the ±290 kHz expected statistically given the ±200 and ±50 kHz uncertainties for the individual infrared[3] and millimeter[16] lines, respectively. This indicates that our estimated measurement accuracy of ±200 kHz is reasonable and probably somewhat conservative.

The present resolution of our spectrometer in the narrow-scan Lamb-dip mode is estimated as follows. The width of the saturation dips in Fig. 5 is 0.7 MHz, obtained with a modulation amplitude of 0.6 V on the laser piezotuner and a cell pressure of 10 mTorr. By reducing the modulation to 0.4 V and lowering the pressure to 7 mTorr, we were able to reduce the dip width to 0.4 MHz without significantly degrading the S/N ratio. Thus, we believe that we can resolve blended features down to a frequency separation of 0.4 MHz.

IV. DISCUSSION

In this work, we have demonstrated wide-span frequency tunability of our dual-mode CO_2-laser/microwave sideband spectrometer via generation of microwave sidebands by hot and sequence band CO_2 laser lines as well as high-J lines of the 9.6-μm-P branch. The spectral gaps between low-J lines have thereby largely been covered, and near-continuous tunability obtained over a 10 cm^{-1} region around the center of the 9.6-μm-regular band. Automated full-sideband microwave sweeps from 6.7–18.5 GHz have been implemented under computer control, with a tracking procedure to maintain optimum tuning of the Fabry–Perot etalon filter throughout a sweep in order to separate a specific sideband from the CO_2 carrier.

In the second mode of operation of our spectrometer, the sidebands have been successfully applied in observations of sub-Doppler saturation-dip spectra for CH_3OH with measurement accuracy of order ±200 kHz. This demonstrates the potential of the instrument for spectroscopy at sub-MHz resolution for molecules with vibrational transition moments comparable to methanol. The frequencies for 33 CH_3OH absorption lines in the C–O stretching band have been measured, adding to the reference data set of accurately known CH_3OH infrared frequencies.[3,12–14] The new lines include a number of K doublets in the ground and first excited torsional states with very small asymmetry splittings that are not accessible with Doppler-limited observations.

The addition of the hot and sequence band lines as well as high-J regular lines to the repertoire of CO_2 laser lines available for sideband generation has significantly improved the spectral coverage of our CO_2-sideband spectrometer and greatly increased its potential for spectroscopic studies, the study of CO_2-pumped far-infrared lasers, and application in pollutant remote sensing.[2] If operation of the laser could also be extended to isotopic CO_2 species such as $^{13}CO_2$, $C^{18}O_2$, and $^{13}C^{18}O_2$ to generate microwave sidebands, this would represent dramatic progress towards the ultimate goal of fully tunable spectral coverage over the whole 9–12 μm midinfrared region.

ACKNOWLEDGMENTS

Financial support of this research by the Canadian Institute for Photonic Innovations and the Natural Sciences and Engineering Research Council of Canada is gratefully acknowledged. M.Y.T. acknowledges partial support from the Russian Fund for Basic Research and the Russian Ministry of Industry, Science and Technologies. Our CO_2 laser is a valued and tangible legacy of the many pioneering contributions of K. M. Evenson to this field, and we wish to dedicate this work to his memory.

[1] P. K. Cheo, IEEE J. Quantum Electron. **QE-20**, 700 (1984).
[2] P. K. Cheo, Z. Chu, L. Chen, and Y. Zhou, Appl. Opt. **32**, 836 (1992).
[3] Z. D. Sun, F. Matsushima, S. Tsunekawa, and K. Takagi, J. Opt. Soc. Am. B **17**, 2068 (2000).

[4] G. Magerl, J. M. Frye, W. A. Kreiner, and T. Oka, Appl. Phys. Lett. **42**, 656 (1983).
[5] G. Pfister, F. Guernet, G. Charton, Ch. Chardonnet, F. Herlemont, and J. Legrand, J. Opt. Soc. Am. B **10**, 1521 (1993).
[6] P. Pracna, K. Sarka, J. Demaison, J. Cosleou, F. Herlemont, M. Khelkhal, H. Fichoux, D. Papousek, M. Paplewski, and H. Burger, J. Mol. Spectrosc. **184**, 93 (1997).
[7] K. M. Evenson, C.-C. Chou, B. W. Bach, and K. G. Bach, IEEE J. Quantum Electron. **30**, 1187 (1994).
[8] A. G. Maki, C.-C. Chou, K. M. Evenson, L. R. Zink, and J.-T. Shy, J. Mol. Spectrosc. **167**, 211 (1994).
[9] Z.-D. Sun, R. M. Lees, L.-H. Xu, M. Yu. Tretyakov, and I. Yakovlev, Int. J. Infrared Millim. Waves **23**, 1557 (2002).
[10] C. Freed and A. Javan, Appl. Phys. Lett. **17**, 53 (1970).
[11] Y.-T. Chan, J. M. Frye, and T. Oka, J. Opt. Soc. Am. B **3**, 935 (1986).
[12] Z. D. Sun, F. Matsushima, S. Tsunekawa, and K. Takagi, J. Opt. Soc. Am. B **16**, 1447 (1999).
[13] Z. D. Sun, S. Ishikuro, Y. Moriwaki, F. Matsushima, S. Tsunekawa, and K. Takagi, J. Mol. Spectrosc. **211**, 162 (2002).
[14] Z. D. Sun, T. Mizuochi, M. Kaneko, F. Matsushima, and K. Takagi, Molecules **8**, 92 (2003).
[15] G. Moruzzi, B. P. Winnewisser, M. Winnewisser, I. Mukhopadhyay, and F. Strumia, *Microwave, Infrared and Laser Transitions of Methanol* (CRC, Boca Raton, FL, 1995).
[16] L.-H. Xu and F. J. Lovas, J. Phys. Chem. Ref. Data **26**, 17 (1997), and references therein.